

Multiwavelength study of Cygnus A II. X-ray inverse-Compton emission from a relic counterjet and implications for jet duty-cycles

Katrien C. Steenbrugge^{1*}, Katherine M. Blundell² and Peter Duffy³

¹*St John's College Research Centre, University of Oxford, St John's College, Oxford, OX1 3JP, UK*

²*University of Oxford, Department of Physics, Keble Road, Oxford, OX1 3RH, UK*

³*UCD School of Mathematical Sciences, UCD, Dublin 4, Ireland*

Accepted . Received

ABSTRACT

The duty-cycle of powerful radio galaxies and quasars such as the prototype Cygnus A is poorly understood. X-ray observations of inverse-Compton scattered Cosmic Microwave Background (ICMB) photons probe lower Lorentz-factor particles than radio observations of synchrotron emission and thus potentially reveal a more aged population. Comparative studies of the nearer and further lobes, separated by many 10s of kpc and thus 10s of thousands of years in light-travel time, yield additional temporal resolution in studies of the lifecycles of such objects. We have co-added all archival *Chandra* ACIS-I data and present a deep 200 ks image of Cygnus A. This deep image reveals the presence of X-ray emission from a counterjet i.e. a jet receding from Earth and related to a previous episode of jet activity. The outer part of this counterjet does not overlay the current counterjet detected in radio emission, excluding the possibility that we detect the current counterjet in X-rays. The non-thermal X-ray emission has a power-law photon index is 1.7, and we interpret this emission as ICCMB radiation. There is an absence of any discernible X-ray emission associated with a jet flowing towards Earth. We conclude that: (1) The emission from a relic jet, indicates a previous episode of jet activity, that took place earlier than the current jet activity appearing as synchrotron radio emission. (2) The presence of X-ray emission from a relic counterjet of Cygnus A and the absence of X-ray emission associated with any relic approaching jet constrains the timescale between successive episodes of jet activity to $\sim 10^6$ years. (3) Transverse expansion of the jet causes expansion losses which shifts the energy distribution to lower energies. Particles with initially high Lorentz factors, that originally gave detectable synchrotron radiation, attain Lorentz factors $\sim 10^3$ and inverse-Compton scatter CMB photons, to give X-ray emission. (4) Assuming the electrons cooled due to adiabatic expansion, the required magnetic field strength is substantially smaller than the equipartition magnetic field strength. (5) A high minimum Lorentz factor for the distribution of relativistic particles in the current jet, of a few 10^3 , is ejected from the central nucleus of this active galaxy.

Key words: galaxies:active–galaxies:individual: Cygnus A–galaxies:jets.

1 INTRODUCTION

The Cygnus A cluster and galaxy (3C 405) are one of the brightest sources in the X-ray sky and have therefore been studied with every major X-ray satellite. In this paper we take advantage of the high spatial resolution of the *Chandra* satellite to study the linear counterjet-like feature this reveals.

The spatial resolution of the ACIS camera onboard *Chandra* allows us to spatially resolve the jet, lobes and hotspots from the central AGN. Therefore one can compare the radio and X-ray properties of a particular galaxy with fine spatial resolution. Cygnus A was observed 11 times with *Chandra*, 10 of which have an expo-

sure time of more than 5 ks, and are used in this paper. Some of the *Chandra* datasets we use have been analysed and published by Wilson et al. (2000), Young et al. (2002), Smith et al. (2002), Bałucińska-Church et al. (2005), Croston et al. (2005), Evans et al. (2006) and Wilson et al. (2006).

One question addressed in this paper relates to the duty cycle of the jet-activity in Cygnus A. That is, of the time for which the super massive black hole central engine in Cygnus A is accreting, for what fraction of that time is matter expelled in the form of relativistic jets? In a recent paper, Nipoti, Blundell & Binney (2005) contended that radio-loudness (manifested by jet activity) in active galaxies such as quasars was analogous to the intermittency of the jet ejection in microquasars, albeit on longer timescales.

Detection of X-ray photons that arise from inverse Compton

* E-mail:kcs@astro.ox.ac.uk

up-scattered Cosmic Microwave Background (ICMB) photons mandates the presence of relativistic particles with Lorentz factors of order 10^3 (Harris & Grindlay 1979). Such particles are likely to have lower Lorentz factors than ambient synchrotron-emitting particles radiating at the typically-observed radio wavelengths, assuming the magnetic field strengths in the lobes of radio galaxies are nT in size or lower. Thus, co-spatial X-rays can reveal information about the lower-energy population of a distribution of relativistic particles than synchrotron radio emission from the same plasma. Furthermore, they can signal the presence of relic (that is previously, but no longer detectable synchrotron emitting) plasma (e.g. Erlund et al. (2006), and Blundell et al. (2006)). Examination of the brightness distribution of ICMB — relative to synchrotron — gives an extra step in temporal resolution in these objects which evolve slowly relative to human timescales.

For a redshift of 0.05607 (Owen et al. 1997) the physical size, i.e. the distance between the outer hotspots not correcting for possible line of sight angle, of Cygnus A is 130 kpc; assuming a cosmology with $H_0 = 73 \text{ km s}^{-1} \text{ Mpc}^{-1}$ and $\Omega_M = 0.3$ and $\Omega_\Lambda = 0.7$. Therefore, the light-travel time between opposite lobes exceeds $\cos \theta \times 4 \times 10^5$ years, where θ is the angle between the axis of the radio source and our line-of-sight. Since the light we observe from opposite lobes is received at the same telescope time, this means that an observer on Earth sees the nearer lobe at a more recent epoch than the further lobe, which is seen at an earlier time in the radio galaxy’s history. Properly accounting for light-travel time effects is important in the interpretation of side-to-side asymmetries in the lobes and jets of quasars and microquasars (e.g. Blundell & Alexander 1994; Miller-Jones et al. 2004).

An important corollary of the different epoch at which we observe different sides of the source is that — relative to the near lobe — we are looking back in time, and attaining an extra, different, step in temporal resolution in these slowly evolving objects.

2 OBSERVATIONS AND DATA REDUCTION

There were 3 observing campaigns on Cygnus A with *Chandra* resulting in 10 observations with an exposure time of at least 5 ks. The details of the observations are listed in Table 1. All observations used the ACIS (Advanced CCD Imaging Spectrometer) instrument. The first 2 observations utilized the ACIS-S, therefore the image of Cygnus A fell on a back-illuminated chip, which has a higher effective area for lower energies. In the second observation a subarray of the CCDs was illuminated, thus allowing for a read-out time of only 0.4 s. This set-up minimizes the pile-up in the core of the AGN. In the other 9 observations the core is seriously piled-up. The last 8 observations are with the ACIS-I configuration and in the VFAINT mode, which gives a reduced background after processing. All the data were obtained from the *Chandra* public archive and reduced (including the thread to obtain the reduced background) with the standard threads (a collection of commands) in CIAO 3.3 (<http://asc.harvard.edu/ciao/threads/>), which included the updated calibration database CALDB 3.2.2. The filtering minimally reduced the exposure times, Table 1 lists the filtered exposure times. The background region was chosen from a low count rate region on the CCD array containing the image of Cygnus A; however, the position of the background region in observation 1 and 2 is different from that of the remaining observations, due to the different instrumental set-up. A circle with radius $14.76''$ centered on $19^h 59^m 41^s .335$ in Right Ascension (J2000) and $+40^\circ 40' 51'' .03$ in Declination (J2000) was used for all but ob-

Table 1. The list of observations of Cygnus A used in this paper, i.e. all *Chandra* observations with an filtered exposure time longer than 5 ks. Listed are the date of the observation, the exposure time as well as the instruments used: ACIS-S or ACIS-I, the mode of observation and ObsID number. See main text for more details.

	date	exposure (ks)	instrument	mode	ObsID
1	2000 05 21	34.72	ACIS-S	FAINT	360
2	2000 05 26	10.17	ACIS-S	0.4 s frame	1707
3	2005 02 15	25.80	ACIS-I	VFAINT	6225
4	2005 02 16	51.09	ACIS-I	VFAINT	5831
5	2005 02 19	25.44	ACIS-I	VFAINT	6226
6	2005 02 21	6.96	ACIS-I	VFAINT	6250
7	2005 02 22	23.48	ACIS-I	VFAINT	5830
8	2005 02 23	23.05	ACIS-I	VFAINT	6229
9	2005 02 25	16.04	ACIS-I	VFAINT	6228
10	2005 09 07	29.65	ACIS-I	VFAINT	6252

servation 2. For the 2nd observation, which has only a strip of the CCDs exposed, a circle centered on $19^h 59^m 46^s .172$ in Right Ascension and $+40^\circ 39' 46'' .06$ in Declination with a radius of $12.3''$ was used.

We aligned the AGN core detected in the 2 – 10 keV band of the first X-ray observation with the fitted coordinates for the 5-GHz core, from observations made by Carilli et al. (1991). The 2 – 10 keV band was chosen to avoid the extended soft X-ray emission detected by Young et al. (2002). Matching the nucleus accurately led to the superposition of the radio and X-ray detected hotspots. This gives us confidence that the radio and X-ray core of the AGN indeed coincide within the resolution of *Chandra*. Using the coordinates determined for the first observation we used the `reproject_aspect` thread to re-align the other 9 observations. This method resulted in an alignment of the core to within $0.5''$ for 7 of the observations, but failed for observations 2 and 6. For observation 2 we did not detect the necessary number of point sources on the strip of the CCDs exposed. A similar problem occurs for observation 6, however, in this case it is due to the short exposure time and not the instrumental set-up. For observation 2 we used AIPS (<http://www.aips.nrao.edu/>) to fit a Gaussian to the core and then matched the position of the peak in emission to that of the radio determined core. This resulted again in an alignment to better than $0.5''$. This method however failed for observation 6; therefore we readjusted the coordinates until alignment was achieved between the pixel with maximum counts in observation 6 and that in observation 1.

Once all 10 X-ray observations were aligned with the 5 GHz radio image, we added the 0.2–10 keV images producing one image for the ACIS-S exposures and one for the ACIS-I exposures using the `merge.all` command in CIAO. We used the first and fifth observations to provide the reference coordinates for the ACIS-S and ACIS-I images respectively. The resulting ACIS-I image, which has the better statistics of the 2 images, is shown with different transfer functions in Figs 1 and 2. For extraction of the spectra from different regions we used the `specextract` command in CIAO. Considering the difference in detector and/or observation mode as well as the time span between the different observations we extracted all the spectra for the different regions for each observation, using the specific `badpixel` file for that observation. The quoted errors on the X-ray luminosity and photon index is for $\Delta\chi^2 = 2$, the RMS of the $\Delta\chi^2$ distribution (or a confidence level of 84.3 % for 1 free

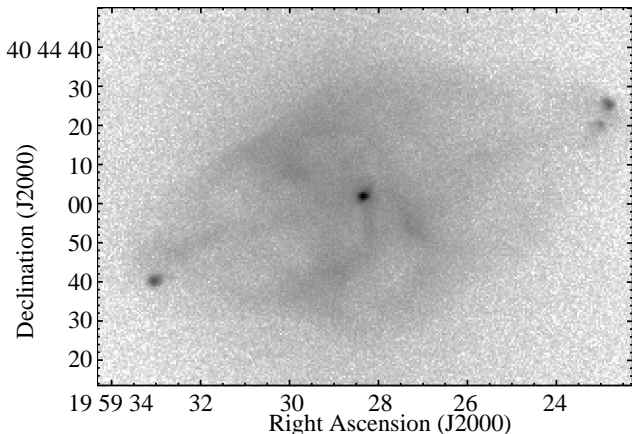


Figure 1. The 0.2–10 keV ACIS-I image of Cygnus A. This image was obtained by adding the last 8 observations listed in Table 1, after reprojecting the files so that the coordinates matched the 5-GHz radio coordinates.

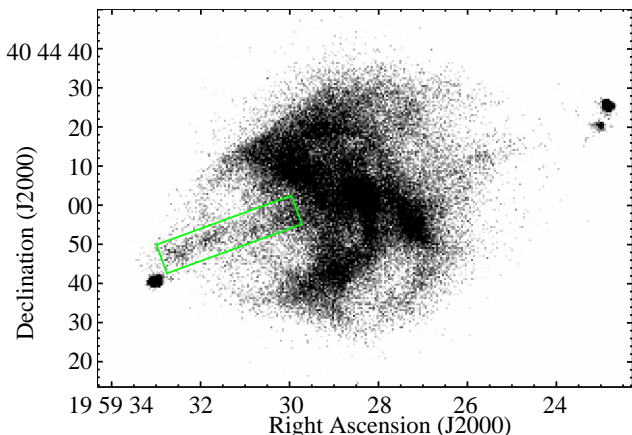


Figure 2. The 0.2–10 keV ACIS-I image, with a different transfer function from that of Fig. 1, clearly showing the linear counterjet-like feature delineated by the green box and the non-detection of anything corresponding to this on the jet side.

parameter) (Kaastra et al. 2004). We used the SPEX (Kaastra et al. 2002) package for fitting the spectra.

3 RESULTS

3.1 X-ray counterjet

Interestingly, a linear counterjet-like feature is easily detected in the 0.2–10 keV image (see Fig. 2), as first reported by Steenbrugge & Blundell (2007). This seems to be most prominent further away from the nucleus and bends at RA=19^h59^m31^s and Dec=+40°43′54″. This bend occurs just inside the two weaker jet knots observed in the 15 GHz radio image (E4 and E5 in Fig. 6 of Steenbrugge & Blundell, accepted companion paper) and between which the counterjet starts to bend over a large angle. We use a box (see Fig. 2) with centre 19:59:31.358 in RA and +40:43:52.54 in Declination, a length of 36.71″ and width of 7.79″ and an angle counter clock-wise of 20° from east to fit the counterjet feature. This is the only significantly detected feature that lies partly within the 5 GHz lobes. Inevitably, the box will contain some emission from the background thermal gas originating from the cluster. The width of the counterjet is $\sim 5''$, and is thus resolved in our *Chandra* image. The width of the brightest knots observed in the 15 GHz image, which have the largest width of the knots in any of the three

radio bands we use, are $\sim 2''.9$ (Steenbrugge & Blundell, accepted companion paper). Thus the X-ray counterjet feature is wider than any radio jet knots in Cygnus A.

3.2 Fitting the X-ray counterjet spectrum

The X-ray counterjet is observed against a bright and variable local background, due to thermal gas in close vicinity of the galaxy. Therefore, we decided to fit this local background as an extra component in our fit to the spectrum of the counterjet, rather than subtracting an unknown local background. The X-ray spectrum of the counterjet (as indicated in Fig. 2), is well fitted (reduced $\chi^2 = 1.1$ for 1582 degrees of freedom) by a power-law with Galactic absorption of $3.5 \times 10^{25} \text{ m}^{-2}$ (Dickey & Lockman 1990). We rebinned the spectrum by a factor of 3, and fitted the spectrum between 0.5–7 keV. The 0.1–10 keV luminosity is $(1.4 \pm 0.2) \times 10^{36} \text{ W}$ or $(7.0 \pm 0.12) \times 10^{35} \text{ W}$ in the 2–10 keV band. The normalization (normalized at 1 keV) is $1.80 \times 10^{51} \text{ photons s}^{-1} \text{ keV}^{-1}$, and the photon index is 1.70 ± 0.02 . There is likely to be contamination of the spectrum by the surrounding hot cluster gas, but the data are too poor to constrain the temperature and normalization of this component, which we fitted as an extra component, using the *cie* model in SPEX. A good indication of the luminosity of this contamination can be obtained from the derived luminosity of the thermal component, fitted together with a power-law, for the jet. The thermal luminosity is $2.1 \times 10^{35} \text{ W}$ in the 2–10 keV range. Fitting the counterjet feature with a thermal model gives a poorer fit, namely a reduced $\chi^2 = 1.2$ (for the same degrees of freedom, for a temperature of 6.3 keV and an emission measure of $5.59 \pm 0.13 \times 10^{71} \text{ m}^{-3}$). Wilson et al. (2006) studied the brighter features, although not the counterjet, in Cygnus A and convincingly showed that the higher temperature gas is at the outer edge, i.e. the contact discontinuity. The gas more centrally located is quite a bit cooler, having temperatures ranging between 3.80 and 4.28 keV and can be explained as being due to the jet break-out phase as modelled by Sutherland & Bicknell (2007a) and Sutherland & Bicknell (2007b). The location of the counterjet-like feature that we observe in the X-rays is not consistent with it either belonging to the gas heated by the jet break-out or the contact discontinuity, a reason why a thermal explanation is less likely.

The spectrum of the counterjet-like feature is in contrast to the mainly thermal spectrum of the other bright, central and curved features clearly seen in Fig. 2. The X-ray counterjet obeys the Bridle & Perley (1984) criteria for jets: its length is more than four times larger than its width; it is separable at high spatial resolution from the surrounding features; and it is aligned with the compact core. Therefore, on the basis of these and its power-law spectrum, we conclude that the long linear feature identified on the east of the source is indeed related to jet activity and not part of the surrounding environment. Furthermore, the counterjet lies on the same line that connects the brighter western hotspot (i.e. the brighter hotspot on the jet side) and the nucleus.

The inner part of the X-ray counterjet does overlie the inner part of the counterjet detected in the radio images, however it does not make the 27°31′ bend observed in the 15-GHz image (Steenbrugge & Blundell, accepted companion paper); rather it extends along its original direction until just north of the bright eastern hotspot. There is a clear gap in emission between the end of the X-ray detected counterjet and the hotspot. We conclude that the X-ray detected counterjet is a relic for the following three reasons: (i) it is extended transversely compared to the radio counterjet and radio jet (as explored in Sect. 4.3), (ii) it does not overlay the outer ra-

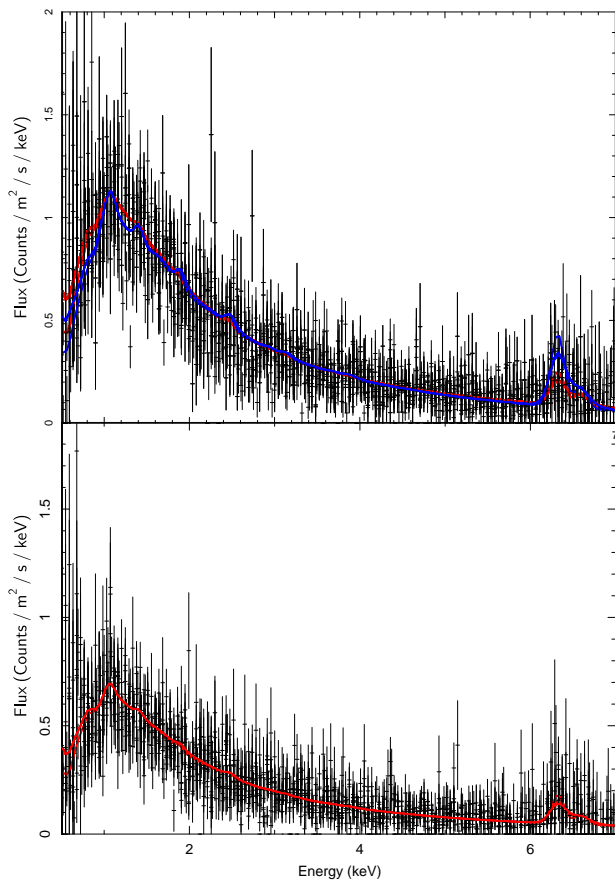


Figure 3. Flux spectra for the energy interval 0.5 – 7 keV from the 10 different observations. *Upper panel:* Spectrum from the counterjet feature within the eastern lobe and the best fit power-law plus thermal model in red. The blue curve indicates the best fit thermal model. Note that the 6.4 Fe $K\alpha$ line is severely overpredicted in this fit. The slight excess around 6.4 keV is due to the thermal emission from the cluster surrounding Cygnus A. The small difference between the fits at shorter wavelengths is a direct result of the different calibrations for the different set-ups of the instruments used. *Lower panel:* Spectrum from a corresponding region on the western lobe where the current jet is observed. The fit to the data shown is a power-law plus thermal model with a spectral slope of 1.75 and temperature of 4 keV. The small differences between the fits at shorter wavelengths and at 6.4 keV is a direct result of the different calibrations and resolution for the different set-ups of the instruments used.

dio counterjet, (iii) there is a gap in emission between the observed counterjet and the hotspots.

The inner part of the relic counterjet overlaps with the inner part of the current counterjet, and therefore we cannot constrain in this region the X-ray luminosity potentially coming from the inner current jet. However, for the outer X-ray counterjet there is a lack of associated 15-GHz radio emission (see fig. 7, Steenbrugge & Blundell, accepted companion paper). This indicates a lack of high Lorentz-factor particles in this relic counterjet compared with those observed in active jets.

3.3 Limits on the density of thermal gas within the lobes

We now consider the possibility of whether the counterjet feature could be explained via thermal emission. We find in Section 3.1

that the emission measure for a thermal plasma is $5.59 \pm 0.13 \times 10^{71} \text{m}^{-3}$. From this emission measure we derive an electron density of $3.1 \times 10^5 \text{m}^{-3}$, assuming $n_e = 2.1n_H$, using $Y = n_e n_H V$ and a volume of $1.22 \times 10^{61} \text{m}^3$. The upper limit to the thermal electron density in the western lobe detected in 5 GHz of Cygnus A is derived by Dreher et al. (1987) to be $4 \times 10^2 \text{m}^{-3}$ for an isotropic random magnetic field from the lack of depolarization observed at eight points in the lobes; this could be higher by as much as two orders of magnitude if the magnetic field has many reversals. Even this extreme upper limit still falls short of the necessary electron density, for the emission to be thermal, by one order of magnitude. This rules out that the feature is due to thermal emission in the lobe. Considering that Cygnus A cluster is a relaxed cluster, showing no sharp, delineated features outside the volume around the Cygnus A galaxy bounded by the lobes and hotspots, we conclude that this feature is unlikely to be thermal, either from the cluster or the gas surrounding the galaxy.

3.4 Limits on X-ray emission from an approaching jet

Tracing the inner part of the jet or counterjet in the X-rays is not straightforward, due to the hot thermal gas surrounding the nucleus and thereby possibly hiding the emission from any inner jet. There is excess X-ray emission centred on Right Ascension= $19^h 59^m 25^s .680$ and Declination= $+40^\circ 44' 12'' .36$, in the western lobe. This feature lies to the north of a jet knot detected at 5 GHz, and therefore is unlikely to be current jet emission. It is located just inside the inner edge of the lobe; a possible explanation for this feature is that X-ray thermal gas is colliding with the back-flowing lobe gas. However, we cannot exclude it being a very faint trace of emission from a relic approaching jet. We conclude that in Cygnus A the current jet is not detected in the 0.2–10 keV X-ray image. We inspected the 6–10 keV image for any evidence of any relic material arising from an approaching jet. There is a slight excess in detected counts just north of the radio jet, overlapping with the lobe. The excess is most pronounced compared with the area just south of the radio jet. We note that there is clear excess of radio emission to the north of the western lobe (see fig 1, Steenbrugge & Blundell, accepted companion paper).

The 3σ upper limit to the 0.1–10 keV luminosity for any approaching jet (see Fig. 3), assuming the spectrum of a relic or current jet is a power-law (corrected for Galactic absorption) is $1.6 \times 10^{35} \text{W}$, which has a best-fit spectral slope of 1.75 ± 0.02 . The box for the jet was centered on RA: $19^h 59^m 25^s .507$ and Dec.: $40^\circ 44' 12'' .76$, with a length of $33.76''$ and the same width as the counterjet box, rotated by 20° . The normalisation of the power-law was $6 \times 10^{50} \text{photons s}^{-1} \text{keV}^{-1}$. A power-law-only fit to the data in the western lobe gives a reduced χ^2 of 1.24 (for 1488 degrees of freedom), while a thermal-only model yields a reduced χ^2 of 1.2 (same d.o.f), while a fit including a thermal and power-law component gives a reduced χ^2 of 1.1 (for 1486 d.o.f). The upper limit to the power-law luminosity is determined by subtracting the luminosity in a box of the same size but offset from the radio detected jet. The width of the box is the same as the width for the box for the detected counterjet. The spectrum obtained from the box centered on the radio jet does show a weak Fe $K\alpha$ emission line, indicating that at least part of the emission is thermal. This is further indication that the flux detected is from the surrounding lobe or cluster and not an approaching jet, or even a relic jet.

Note that this upper limit to the jet luminosity is rather large, due to the presence of hot gas surrounding the Cygnus A galaxy

from the intracluster gas. This upper limit is only a quarter of the luminosity detected for the counterjet.

3.5 Other bright features in the X-ray image

Figs. 1 and 2 clearly show that there are several bright extended regions (besides the counterjet, the hotspots and the nucleus) which are well fitted with a thermal component. This is completely consistent with the results obtained by Wilson et al. (2006). A thorough analysis of the bright extended thermal emission is given by Wilson et al. (2006) and Smith et al. (2002). Therefore we can exclude ICCMB as the emission mechanism for these bright regions. In a future paper, we will discuss the thermal features of the X-ray emission associated with Cygnus A in detail. The structure of these bright features is consistent with having either originated in the shock break-out of the jet as modelled by Sutherland & Bicknell (2007a) and Sutherland & Bicknell (2007b) or being the contact discontinuity as studied by Wilson et al. (2006).

3.6 Comparison with other X-ray detected jets and lobes

We do not detect in the X-ray image of Cygnus A any of the jet knots observed in the different radio bands, either in the jet or the counterjet. Moreover, the X-ray counterjet-like feature has a slowly varying brightness distribution along its length, in contrast with the well-studied knotty X-ray emission from jets generally attributed to synchrotron radiation, and perhaps more in keeping with what might be expected for ICCMB.

Pictor A is the only other radio galaxy with a possible detected X-ray counterjet. Hardcastle & Croston (2005) explain this weak counterjet emission as synchrotron emission, because the X-ray flux ratio between the jet and counterjet is about 6; and the X-ray spectrum of the counterjet is steep. In Pictor A the X-ray jet is clearly more luminous than the counterjet, contrary to the case in Cygnus A. In Pictor A there is no indication of a radio counterjet in VLBI observations (Tingay et al. 2000). For Cygnus A Krichbaum et al. (1998) do detect the VLBI counterjet.

The relative smoothness of the X-ray emission coming from the counterjet is is very different from, for example, 3C 303 (an unusual double radio source, Kataoka et al. (2003)), 4C 19.44 (a Seyfert 1 galaxy according to Simbad, Sambruna et al. (2002)), Cen A (prototypical FR I radio galaxy, Kraft et al. (2002)), and M 87 (an FRI, Marshall et al. (2002)), where in the X-rays individual knots are clearly seen and the brightness of the jet is rather variable but much less luminous. Furthermore, in these jets, the knots closest to the nucleus are in general the brightest in X-rays and the emission is generally attributed to the synchrotron mechanism. In contrast, in Cygnus A the brightness is not much weaker at the furthest end of the counterjet. A further discussion of these important differences is deferred to a future paper.

For a number of radio galaxies, the counterlobe is brighter in X-rays than the lobe (Brunetti et al. (2001); Brunetti et al. (2002); Sambruna et al. (2002); Bondi et al. (2004)). The asymmetric brightness is explained as inverse-Compton (IC) emission, due to anisotropic scattering of infrared and optical photons from the nucleus (Brunetti et al. 1997). In all these cases the brightness of the X-ray lobe falls off steeply with increasing distance from the nucleus. Furthermore, the luminosity asymmetry is a strong function of the inclination angle, and the counterjet needs to be inclined to the line of sight by a rather large angle to see this effect clearly. According to Brunetti et al. (1997), the IC emission from the

counterlobe in Cygnus A should be small compared to the thermal component, and that is indeed consistent with our analysis of the (counter)lobe spectra.

4 DISCUSSION

4.1 Mechanism for generation of ICCMB and implications for the low-energy turnover

The upper limit of ICCMB associated with the current episode of jet activity (either from the jet or the counterjet) together with the presence of ICCMB associated with previous jet activity, implies an upper limit to the number density of 10^3 Lorentz factor particles. This, together with the clearly evident current jets emitting radio synchrotron, suggests that the current synchrotron jet plasma has a low-energy turnover above 10^3 in the distribution of Lorentz factors of the plasma ejected from close to the black hole.

However, the absence of ICCMB from the current jet could potentially be due in part to X-ray bright galaxy/cluster emission. The upper limit to the X-ray brightness of the jet is just a quarter of that of the counterjet luminosity, implying that the number density of particles with Lorentz factors $\sim 10^3$ is less than a quarter in the current jet compared with that in the observed relic counterjet. The upper limit for the current jet is still about 450 times brighter than the jet in Cen A, so a current jet of similar luminosity will have gone undetected, as would the current counterjet. However, the emission mechanism of the Cen A jet is synchrotron emission, therefore sampling much higher Lorentz factor particles.

4.2 Light-travel time effects and cooling

The observation of X-ray emission from the counterjet side, and the absence of such emission from the approaching side of the source, places general constraints on the rate at which the X-ray emission must decline which, assuming symmetrical conditions, depends purely on light-travel time arguments. We consider approaching and receding jets moving with speed $v = \beta_{\text{HS}}c$ from the central source and making an angle θ with the observer's line of sight. When the approaching jet is observed to have extended out to a distance d , so that $t_{\text{app}} = d/v$ is the time since the jet started advancing, we will observe emission from the furthest extremity of the receding jet. The extremity, i.e. hotspot, of the receding jet is observed at a younger age than that at the closest point to us of the approaching jet, with the ratio of ages (t_{rec} and t_{app}) given by

$$t_{\text{rec}} = \left(\frac{1 - \beta_{\text{HS}} \cos \theta}{1 + \beta_{\text{HS}} \cos \theta} \right) t_{\text{app}}. \quad (1)$$

Therefore, the difference in age between the observed jet extremities, which must of course be imaged at the same "telescope time", is

$$\Delta t = \frac{2\beta_{\text{HS}} \cos \theta}{1 + \beta_{\text{HS}} \cos \theta} t_{\text{app}}. \quad (2)$$

What we actually observe is not just dependent on the kinematics of light-travel time, but also on the evolution of the luminosity in the jet material. To illustrate this point we consider the simple case where the X-ray, ICCMB emission depends on the time since emission from the central source in a manner qualitatively illustrated in Fig. 4.

In this picture the relic jet/counterjet plasma is moving at speed β_{pl} ; this is very likely to be slower than the speed at which

the current jet or hotspots move otherwise we would not see any relic plasma along the counterjet. X-rays are emitted at a steady rate for a period of time and then cool or fade over a timescale t_{cool} . When the cooling is sufficiently rapid, then the cooling timescale $t_{\text{cool}} < \Delta t$, and the leading edge of the forward jet will be observed to cool and fade before the far extremity of the counterjet is observed to cool. However, the details depend on the rate at which X-ray ICCMB fades during the cooling epoch and in the plasma rest frame. Doppler boosting also plays a role, acting to enhance the approaching emission relative to that which is receding. The ratio of intensities for approaching and receding jets is dependent on the flux density, $S_\nu \propto \nu^{-\alpha}$, with $\alpha \approx 0.7$. We consider the flux ratio between equal volumes of plasma at either extremity of the approaching and receding jets,

$$\frac{S_{\text{app}}}{S_{\text{rec}}} = \left(\frac{1 + \beta_{\text{pl}} \cos \theta}{1 - \beta_{\text{pl}} \cos \theta} \right)^{3+\alpha} \frac{L_{\text{app}}(t_{\text{app}})}{L_{\text{rec}}(t_{\text{rec}})} \quad (3)$$

where we have ignored factors $O(\beta_{\text{pl}}^2)$.

Initially, when neither jet has started to fade, the forward jet will be more luminous on the basis of size relative to the receding jet and Doppler boosting. Subsequently, in the relic phase, both jets will expand in their own rest frame and the Doppler boosting will be modified according to the decaying, power-law spectrum and any deceleration of the emitting material. Then, as shown in Fig. 4, the forward jet will be observed to fade first and the flux ratio will be observed to decline, giving a much more prominent counterjet. We measure the flux ratio for the relic jet over the relic counterjet in the 2-10 keV band to be less than 0.25, as the upper limit to any jet emission is about 4 times smaller than the measured counterjet emission. From the total observed length of the radio source of 130 kpc, we calculate (assuming $\theta = 60^\circ$) that the light travel-time difference between the hotspots is 2×10^5 years. Therefore the cooling time needs to be $\lesssim 10^5$ years. Thus, provided that the intrinsic luminosity of X-ray ICCMB declines quickly enough during cooling that it takes place in a light-crossing time (2×10^5 years), the system will always evolve to a state where the receding jet has a greater X-ray luminosity than the older, approaching counterpart. This cooling timescale places a constraint on the particular cooling mechanism for the jet which we consider in the next section.

4.3 Cooling mechanism for the jet

We require a mechanism that can produce a broad, X-ray counterjet with a low energy turnover $\gamma \lesssim 10^3$ needed to explain the ICCMB emission. The luminosity is required to decline in order to explain the absence of an approaching X-ray jet in 2×10^5 years, by a factor of four or more. With radio observations of an approaching radio jet as motivation, we would expect the relic X-ray counterjet to have had a thinner, radio jet as progenitor, containing a higher low-energy turnover. We consider two extreme cases for the possible mechanism, first that the electrons in the radio jet escape diffusively into the lobe and second that the jet expands adiabatically.

The diffusive escape of electrons from a radio jet of width L would occur over a timescale of order L^2/D where D is the diffusion coefficient. Assuming that Bohm scattering is valid, we take the particle mean free path to be equal to its gyroradius so that $t_{\text{escape}} \approx R^2/(r_{\text{g}}c)$, where R is the radius of the relic jet width and r_{g} is the gyro-radius. With $R \approx 7.5 \times 10^{19}$ m and $B \approx 10^{-9}$ T such an escape time would be many orders of magnitude greater than a Hubble time so that diffusive escape could only deplete a radio jet of synchrotron emitting electrons if their mean free path

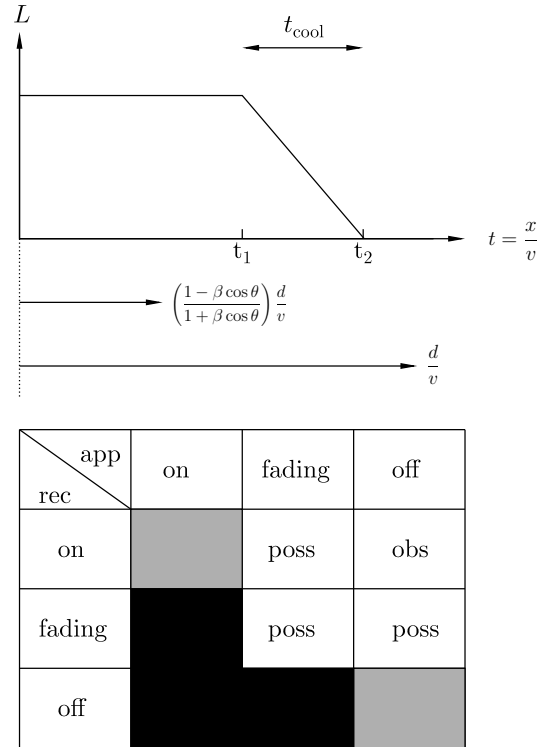


Figure 4. *Upper:* This is a schematic lightcurve for a fading jet. *Lower:* This illustrates the possible combinations of on/off states for the fading jet and counterjet. The squares coloured black are not formally possible, because of light-travel time effects while those in grey are formally possible but excluded for this object by observation. The square labelled “obs” is the case we study in the text.

greatly exceeded the gyroradius. A further problem with any model based on diffusive escape is that it would provide no natural means of reducing the Lorentz factors of energetic particles and/or magnetic fields, needed to convert the plasma from a radio-synchrotron emitter to one dominated by X-ray ICCMB.

An alternative model, which may work on sufficiently short timescales, is that the radio jet simply expands adiabatically into the lobe. This will reduce the particle energies and the magnetic field strength leading to a decline in the radio synchrotron emission. The low-energy turnover will also move to lower Lorentz factors, ultimately producing sufficient $\gamma \sim 10^3$ particles needed for observable X-ray ICCMB emission between 0.1 keV and 10 keV. Observationally the X-ray counterjet has expanded in volume by roughly a factor of four when compared with the younger radio jet. Under adiabatic expansion $PV^{4/3}$ is constant, for material dominated by relativistic particles; the factor of $4^{4/3}$ is plausible for the pressure ratio between radio lobe and X-ray emitting material supporting the adiabatic expansion model. While there is obviously scope for detailed modelling of the X-ray counterjet, including the details of how the expansion takes place and the possible excitation of shocks, it is encouraging that the simple model of adiabatic jet expansion into the lobe is consistent with the new observations presented in this paper.

The X-ray emission and upper limit to the radio flux allow us to make estimates of both the number density of relativistic electrons and the mean magnetic field. In the X-ray counterjet we take

the differential electron spectrum, per unit volume, to be a power law above a low-energy turnover γ_{\min}

$$N(\gamma) = N_0 \left(\frac{\gamma}{\gamma_{\min}} \right)^{-p}, \quad \gamma \geq \gamma_{\min} \quad (4)$$

where we have normalised our spectrum such that N_0 is the differential number of particles, per unit volume, at $\gamma = \gamma_{\min}$. The observed X-ray counterjet luminosity between photon energies of 0.1keV and 10keV is $L_X = 1.4 \times 10^{36}$ W from a volume $V \approx 1.22 \times 10^{61} \text{ m}^3$. When the source of this emission is inverse Compton scattering, by the power law distribution of electrons, of the Cosmic Microwave Background, we can place a constraint on the values of N_0 and γ_{\min} (Rybicki & Lightman (1986), section 7.3 and equation 7.31).

$$L_X \approx 1.4 \times 10^{36} \text{ W} \left(\frac{N_0}{4.3 \times 10^{-2} \text{ m}^{-3}} \right) \left(\frac{\gamma_{\min}}{10^3} \right)^p \quad (5)$$

where $p = 2.4$. This value for N_0 determines the energy density, e , in energetic electrons and the equipartition magnetic field ($B_{\text{equip}}^2/2\mu_0 = e$, giving

$$\left(\frac{B_{\text{equip}}}{1 \text{ nT}} \right) \approx 1.48 \times 10^2 \left(\frac{N_0}{4.3 \times 10^{-2} \text{ m}^{-3}} \right)^{1/2} \left(\frac{\gamma_{\min}}{10^3} \right). \quad (6)$$

However, the upper limit to the radio emission from the relic region also places constraints on the magnetic field and the particle spectrum. With a lower cut-off to the energetic electron distribution there will be a minimum frequency to synchrotron radiation given by

$$\left(\frac{\nu_{\min}}{8 \text{ GHz}} \right) \approx 5 \times 10^{-3} \left(\frac{\gamma_{\min}}{10^3} \right)^2 \left(\frac{B}{1 \text{ nT}} \right). \quad (7)$$

The upper limit to the flux density from the relic X-ray counterjet regions is $P_\nu = 2.048 \times 10^{24} \text{ W Hz}^{-1}$ at a frequency of 8 GHz, and this places a constraint on the field and spectrum, determined by standard synchrotron radiation formulae (Longair 1994)

$$\left(\frac{B}{1 \text{ nT}} \right)^{(p+1)/2} \left(\frac{N_0}{4.3 \times 10^{-2} \text{ m}^{-3}} \right) \left(\frac{\gamma_{\min}}{10^3} \right)^p < 1.37 \times 10^{-2} \quad (8)$$

With the product $N_0 \gamma_{\min}^p$ fixed by the observation of X-ray ICCMB we find the important result that the actual mean B field in the relic region is much smaller than that required for equipartition

$$B \approx 10^{-4} B_{\text{equip}}. \quad (9)$$

Therefore, if the jet material was initially created with approximate equipartition between field and particles, it is clear that the magnetic field energy is dissipated more quickly than that of the particles as the jet evolves into the relic phase. Clearly there are two important problems here; firstly whether, and how, the particles and field are produced in equipartition and secondly how their respective energy densities are dissipated. Detailed consideration of these issues are beyond the scope of this paper but are the subject of ongoing simulations for relativistic flows (Reville et al. 2007; Spitkovsky 2008).

4.4 Jet duty-cycle characteristics

Taking the difference in light travel time to be 2×10^5 years, an (assumed constant) value of the hotspot advance speed of 0.1 c and using equation 2, gives a timescale of 10^6 years since the previous jet activity.

4.5 Intermittency and relic jets in quasars and radio galaxies

Nipoti et al. (2005) explored the intermittency, hence duty cycle, of jet activity (“flaring events”) in microquasars. They suggested that if there is a good analogy between microquasars and quasars, that intermittency should also be seen in the jet activity of quasars and radio galaxies. Indirect evidence the authors cited for this analogous behaviour is the similarity of the duty cycle of microquasar jets with the fraction of quasars that are radio-loud. A specific test of this prediction is that there should be evidence of previous/relic jet activity in some quasars and radio galaxies.

The existence of relic jet-activity in Cygnus A, revealed via ICCMB emission, indicates that there was an epoch of jet activity earlier than the current synchrotron radio jet. The age of the current radio jet is of order 10^6 years (Steenbrugge & Blundell, accepted companion paper). There is no evidence of a bright compact radio feature (e.g. resembling a hotspot) at the end of the relic X-ray counterjet indicating there has been a pause between the two jet episodes. The fading timescale for synchrotron emission from radio lobes is $\lesssim 10^6$ years (Blundell & Rawlings 2000), longer than the light-travel time from the furthest extremity of Cygnus A to the nearest.

Strong indications of episodic jet activity and re-starting jets have been observed in the case of the so-called double-double radio galaxies. For example, Schoenmakers et al. (2000) derive an “interruption timescale” of a few 10^6 years between successive jet ejections.

Why has a jet-cooling timescale not been established in other sources? There are at least two reasons: (i) the duty cycle may be shorter in other sources than in Cygnus A and (ii) the lack of suitably deep observations. We remark that the X-ray brightness of the relic X-ray counterjet of Cygnus A, if it were redshifted to $z = 0.5$ and $z = 1$ respectively would be 0.16 and 0.079 of the observed luminosity at redshift 0.057. To observe a relic counterjet at these higher redshifts the exposure time would need to be increased by factors 9 and 18 compared to the current 200 ks ACIS-I exposure time.

Nonetheless there are perhaps two other instances of a previous epoch of jet activity in a powerful radio quasar being revealed by ICCMB, rather than by lobe emission as in the case of the double-double radio galaxies. The quasars are 3C 294 where the current radio axis is offset slightly from a faint X-ray axis (Fig. 4 of Erlund et al. (2006)) and is offset significantly from the bright X-ray axis (Fig. 2 Erlund et al. (2006)); another possible example is 3C 356 (Crawford & Fabian 1993).

5 CONCLUSION

We have analysed the X-ray counterjet revealed by the combined 200 ks *Chandra* ACIS-I and ACIS-S observations of Cygnus A. Its power-law spectrum, with photon index of 1.7, indicates that the feature is unlikely due to thermal gas, and is therefore probably due to emission from jet plasma having spectral index 0.7. Comparing the X-ray detected counterjet with the observed radio counterjet in the 5-GHz and 15-GHz radio images, we conclude that the counterjet detected in X-rays is a relic jet. This conclusion was reached from the following observations: (i) the curvature of the outer parts of the X-ray counterjet is significantly different from that of the current radio counterjet; (ii) this feature lacks any directly associated radio emission implying a lack of high energy synchrotron particles; and (iii) the width of the X-ray counterjet is significantly broader than the radio jet or counterjet implying expansion.

From the non-detection of an approaching X-ray (relic) jet, and the light travel-time difference between the approaching and receding hotspots, we find that the likely interval between the current and previous episodes of jet activity is $\sim 10^6$ years and that the cooling time of the jet has to be less than 2×10^5 years. This short timescale can plausibly be explained by adiabatic expansion causing the jet to cool and thereby fade in the X-rays. The upper limit for observed radio emission due to the relic counterjet allows us to deduce an upper limit for the magnetic field strength within it; this is well below the equipartition value. Our non-detections of X-ray emission from the current jets, but the presence of X-ray emission from a relic jet, indicates that there is a turnover in the energy distribution of the jets ejected from the nucleus of Cygnus A. The jet emerging from the nucleus, is characterized by particles with Lorentz factors, $\gamma \gtrsim 10^3$.

ACKNOWLEDGMENTS

KCS would like to thank St John's College, Oxford for a fellowship; KMB expresses her gratitude to the Royal Society and PD thanks the Royal Irish Academy.

REFERENCES

- Bałucińska-Church M., Ostrowski M., Stawarz Ł., Church M. J., 2005, *MNRAS*, 357, L6
- Blundell K. M., Alexander P., 1994, *MNRAS*, 267, 241
- Blundell K. M., Fabian A. C., Crawford C. S., Erlund M. C., Celotti A., 2006, *ApJL*, 644, L13
- Blundell K. M., Rawlings S., 2000, *AJ*, 119, 1111
- Bondi M., Brunetti G., Comastri A., Setti G., 2004, *MNRAS*, 354, L43
- Bridle A. H., Perley R. A., 1984, *ARAA*, 22, 319
- Brunetti G., Bondi M., Comastri A., Setti G., 2002, *A&A*, 381, 795
- Brunetti G., Cappi M., Setti G., Feretti L., Harris D. E., 2001, *A&A*, 372, 755
- Brunetti G., Setti G., Comastri A., 1997, *A&A*, 325, 898
- Carilli C. L., Perley R. A., Dreher J. W., Leahy J. P., 1991, *ApJ*, 383, 554
- Crawford C. S., Fabian A. C., 1993, *MNRAS*, 260, L15
- Croston J. H., Hardcastle M. J., Harris D. E., Belsole E., Birkinshaw M., Worrall D. M., 2005, *ApJ*, 626, 733
- Dickey J. M., Lockman F. J., 1990, *ARAA*, 28, 215
- Dreher J. W., Carilli C. L., Perley R. A., 1987, *ApJ*, 316, 611
- Erlund M. C., Fabian A. C., Blundell K. M., Celotti A., Crawford C. S., 2006, *MNRAS*, 371, 29
- Evans D. A., Worrall D. M., Hardcastle M. J., Kraft R. P., Birkinshaw M., 2006, *ApJ*, 642, 96
- Hardcastle M. J., Croston J. H., 2005, *MNRAS*, 363, 649
- Harris D. E., Grindlay J. E., 1979, *MNRAS*, 188, 25
- Kaastra J. S., Mewe R., Raassen A. J. J., 2002, *Proc. Symp. New Visions of the X-ray Universe in the XMM-Newton and Chandra era*
- Kaastra J. S., Tamura T., Peterson J. R., Bleeker J. A. M., Ferrigno C., Kahn S. M., Paerels F. B. S., Piffaretti R., Branduardi-Raymont G., Böhringer H., 2004, *A&A*, 413, 415
- Kataoka J., Edwards P., Georganopoulos M., Takahara F., Wagner S., 2003, *A&A*, 399, 91
- Kraft R. P., Forman W. R., Jones C., Murray S. S., Hardcastle M. J., Worrall D. M., 2002, *ApJ*, 569, 54
- Krichbaum T. P., Alef W., Witzel A., Zensus J. A., Booth R. S., Greve A., Rogers A. E. E., 1998, *A&A*, 329, 873
- Longair M. S., 1994, *High energy astrophysics. Vol.2: Stars, the galaxy and the interstellar medium*. Cambridge: Cambridge University Press, —c1994, 2nd ed.
- Marshall H. L., Miller B. P., Davis D. S., Perlman E. S., Wise M., Canizares C. R., Harris D. E., 2002, *ApJ*, 564, 683
- Miller-Jones J. C. A., Blundell K. M., Duffy P., 2004, *ApJL*, 603, L21
- Nipoti C., Blundell K. M., Binney J., 2005, *MNRAS*, 361, 633
- Owen F. N., Ledlow M. J., Morrison G. E., Hill J. M., 1997, *ApJL*, 488, L15+
- Reville B., Kirk J. G., Duffy P., O'Sullivan S., 2007, *A&A*, 475, 435
- Rybicki G. B., Lightman A. P., 1986, *Radiative Processes in Astrophysics*. *Radiative Processes in Astrophysics*, by George B. Rybicki, Alan P. Lightman, pp. 400. ISBN 0-471-82759-2. Wiley-VCH, June 1986.
- Sambruna R. M., Maraschi L., Tavecchio F., Urry C. M., Cheung C. C., Chartas G., Scarpa R., Gambill J. K., 2002, *ApJ*, 571, 206
- Schoenmakers A. P., de Bruyn A. G., Röttgering H. J. A., van der Laan H., Kaiser C. R., 2000, *MNRAS*, 315, 371
- Smith D. A., Wilson A. S., Arnaud K. A., Terashima Y., Young A. J., 2002, *ApJ*, 565, 195
- Spitkovsky A., 2008, *ApJL*, 673, L39
- Steenbrugge K. C., Blundell K. M., 2007, *Ap&SS*, 310, 321
- Sutherland R. S., Bicknell G. V., 2007a, *Ap&SS*, pp 325–+
- Sutherland R. S., Bicknell G. V., 2007b, *ArXiv e-prints*, 707
- Tingay S. J., Jauncey D. L., Reynolds J. E., Tzioumis A. K., McCulloch P. M., Ellingsen S. P., Costa M. E., Lovell J. E. J., Preston R. A., Simkin S. M., 2000, *AJ*, 119, 1695
- Wilson A. S., Smith D. A., Young A. J., 2006, *ApJL*, 644, L9
- Wilson A. S., Young A. J., Shopbell P. L., 2000, *ApJL*, 544, L27
- Young A. J., Wilson A. S., Terashima Y., Arnaud K. A., Smith D. A., 2002, *ApJ*, 564, 176